# Dispersion and Percolation Transitions of Nanorods in Polymer Solutions

**Megha Surve, Victor Pryamitsyn, and Venkat Ganesan***

*Department of Chemical Engineering, University of Texas at Austin, Austin, Texas 78712*

*Received July 17, 2006; Revised Manuscript Received November 2, 2006*

ABSTRACT: We study the effective pair interaction potentials and the resulting phase behavior, percolation transitions of nanorods dispersed in solutions of adsorbing polymers. We use polymer self-consistent-field theory in conjunction with the Derjaguin approximation to compute the polymer-mediated orientation-dependent pair interaction potential between cylindrical nanorods. A modified Flory theory and a simple analytical model are used to delineate the different equilibrium phases and the onset of percolation for nanorods in polymer solutions. Our results suggest that the topology of the phase diagram of a mixture of polymer and rods is highly dependent on the anisotropy of the rods, relative sizes of the rods and polymers, concentration of the polymer, and the strength of adsorption. For the case of nonadsorbing polymers, the polymer depletion-induced attractive interactions result in a large two-phase region which widens with an increase in the polymer concentration. Addition of adsorbing polymers is observed to lead to a richer phase behavior where at high polymer concentrations the polymer-induced repulsive interactions result in steric stabilization of the particles and lead to an isotropic−nematic transition which closely resembles the behavior for hard rod suspensions. As a model mimicking nanotube−polymer mixtures, we also discuss the influence of strong rod−rod van der Waals interactions on the stability characteristics.

## I. Introduction

Polymers have been commonly used in a number of technological applications to control the stability of colloidal suspensions. The ability of polymers to stabilize colloidal materials has been shown to depend strongly on the specific interactions between the polymer and the particles. For instance, for the case of a polymer with no preferential interactions (nonadsorbing) with the particles, an effective attraction of purely entropic origin is induced between the particles.[1−3] The latter typically results in demixing and phase separation of the colloid−polymer mixture. For the case of polymers that can adsorb onto the particles, the effective interparticle interactions range from being strong attractions at low polymer concentrations and/or adsorption strengths, to purely repulsive interactions at high polymer concentrations and/or adsorption strengths.[4−6] These characteristics can lead to a rich phase behavior of the colloid−polymer mixture such as phase separation, reentrant miscibility, etc.[7,8] Finally, when the polymer is grafted onto the particles, the excluded volume repulsions between tethered chains result in a net repulsion between the polymer coated particles, which stabilizes colloidal dispersions.[9] For the case of dispersions of spherical colloidal particles, the interparticle interactions and the resultant phase behavior of particles in the presence of nonadsorbing, adsorbing, and grafted polymers have been the subject of many experimental, theoretical, and simulation studies and are fairly well understood.

In the case of dispersions of anisotropic particles such as platelets, cylindrical rods, ellipsoids, etc., the aspect ratio becomes an important consideration in determining the phase behavior. Early theoretical works of Onsager[10] and Flory[11,12] clarified the concentration driven isotropic−nematic transition in thermotropic hard rod dispersions. Onsager's theory[10] truncates a virial expansion for the free energy at the second virial level and finds the equilibrium state of the system by a functional minimization of free energy with respect to angular distribution of rods. In contrast, Flory theory[11,12] derives the equilibrium orientational distribution of rods such that the combinatorial partition function (equivalent to the entropy of the orientational distribution) of the rods is maximized. The predictions of these theories have been found in approximate agreement with experiments on synthetic as well as naturally occurring rodlike polymers.[13−16] Most developments that have followed later have incorporated additional interactions into the original Onsager's and Flory's theories to predict the occurrence of other orientationally and/or translationally ordered phases.[17−20]

Despite the above theoretical progress, the effects of an added polymer on the interactions between anisotropic particles and their resultant phase behaviors are comparatively unexplored. The case of polymer-induced depletion attractions and their effect on the stability of dispersions of rodlike particles have recently been studied by using a second virial approximation,[21] scaled particle theories,[19] Monte Carlo simulations,[22] etc. However, a recent surge in the applications for anisotropic particles such as carbon nanotubes, nanofibers, clay particles, etc., has drawn much attention to the role of an added, *adsorbing* polymer in controlling the stability of dispersions of anisotropic particles.[23] Generally, many such systems are characterized by strong van der Waals attractions between the pristine nanofillers which lead to the formation of aggregates and bundles of the filler particles.[23−25] The latter diminishes the dimensional advantage of nanosized fillers and currently proves to be a big hurdle in realizing the predicted theoretical limits for property enhancements in many cases. To counter this, a variety of different approaches such as surfactant adsorption,[26−28] covalent modification,[29−31] block copolymer grafting,[32,33] etc., have been developed to induce short-range repulsions between the filler particles so as to prevent their aggregation. An equally attractive strategy that has emerged in this context is the addition of nonspecific, albeit adsorbing, polymers to facilitate the isolation and dispersion of the individual filler particles.[23] In such cases, the induced repulsions due to polymer adsorption are speculated

* To whom all correspondence should be addressed.

10.1021/ma061603j CCC: $37.00 
Published on Web 12/14/2006

to prevent aggregation arising from the strong short-range van der Waals attractions.[33] Instances of this strategy have been reported in experiments where the addition of adsorbing polymers such as poly(methyl methacrylate), poly(vinylpyrrolidone), DNA, etc., facilitates a dispersion of carbon nanotubes.[23,34−37] However, only limited theoretical work exists on the phase behavior of rodlike particles in the presence of adsorbing polymers and the effects of polymer−rod preferential interactions on these characteristics.

In many of above applications, beyond achieving a stable dispersion, obtaining a stable "percolated" network of the fillers proves equally important.[24,25,38,39] For instance, dispersing anisotropic filler particles in a polymeric matrix transforms the linear viscoelastic properties of composites from liquidlike characteristics to a solidlike behavior at very low filler loadings.[40] These changes in the rheological properties have been attributed to formation of percolated filler networks in the polymeric matrix. Similar effects have been observed in the context of electrical conductivity of polymer−CNT composites, where beyond a threshold volume fraction of fillers the electrical conductivity of the composites increases by several orders of magnitude.[41] This abrupt change in the conductivity is again attributed to formation of percolated structures of filler particles. Finally, recent experiments by Kashiwagi et al.[42] have demonstrated a close relationship between fire retarding properties of nanocomposites and the formation of percolated structures of filler particles. There has again been only limited theoretical work[43] characterizing the role and impact of polymer matrix upon the percolation thresholds.

In this article, we present results on the effects of polymer−particle interactions, the concentration of polymer, the radius of rods and the aspect ratio of rods on the adsorption characteristics, the phase behavior, and percolation thresholds for nanorods dispersed in polymer solutions. As model for the pristine system, we consider the case of simple hard rods and limit ourselves to the isotropic−nematic transition in such a system. We use the framework of self-consistent-field theory for polymers to derive the pair interaction potentials between flat surfaces in polymer solutions.[44] These are used in a modified Derjaguin approximation[45,46] to deduce the interactions between cylindrical rods. This approximation does introduce some inaccuracies when the size of the rods in smaller than the range of the interactions; however, the qualitative results obtained within this framework are expected to be accurate. We then follow an approach similar to that proposed by Flory[17,18] to predict the isotropic−nematic transition for the rodlike particles, now interacting through these "polymer mediated effective interaction potentials". At finite volume fractions of rods, the multibody effects can result in considerable change in the overall concentration of polymer and can be accounted through a method discussed in our earlier work (section VA of ref 6). However, for dilute particle concentrations, such effects are expected to be small, and we examine the phase behavior based on pair interactions potentials computed at the infinite dilution of rods. Further, we use a simple analytical approach to also predict the percolation thresholds for the rods in the presence of such polymer-induced interactions. We also discuss effect of adsorbing polymer on the stability of dispersions of rods characterized by strong van der Waals interactions (the latter serving as a model for nanotubes).

Our results predict that the addition of moderately and strongly adsorbing polymers can result in a stabilization of the dispersions of rods. In this context, an increase in either the polymer concentration and/or the strength of adsorption is shown to favor the formation of stable isotropic phases. Similar conditions are also shown to favor the formation of stable percolated structures. In contrast, at lower adsorption strengths and/or lower polymer concentrations, the percolation transitions are observed to occur within phase-separated region. The topology of phase diagrams and the location of percolation lines are also shown to be strongly dependent on the radius of the rods (relative to the polymer size) and the aspect ratio of rods.

The rest of the article is arranged as follows: In section II, we provide more details of the approach used to derive the polymer-mediated effective interactions between rodlike particles and the corresponding extension of Flory theory for isotropic−nematic transition to incorporate such interactions. We also explain the idea behind the model used to study percolation transitions in a system of interacting rodlike particles. Section III presents the phase diagrams for the mixtures of polymer and nanorods with emphasis on the roles of polymer−particle interaction strength, polymer concentrations, the radius of rods, and aspect ratio of rods. In section IV, we analyze the effect of above parameters on the percolation transition of rods. In section V, we briefly discuss the influence of adsorbing polymers upon the stability of dispersions of rods characterized by strong van der Waals interactions. In section VI, we discuss our results in the context of the experimental observations for nanorod−polymer mixtures. We conclude with a brief summary and outlook in section VII.

## II. Modeling Framework

**A. Pair Interactions for Rodlike Particles.** We first outline the approach followed to obtain the polymer-mediated pair interaction potentials between nanorods dispersed in polymer solutions. The framework consists of three steps: (i) use of self-consistent-field theory to derive the polymer-mediated pair interaction potentials between flat surfaces; (ii) use of the Derjaguin approximation to obtain the interactions between parallelly oriented rodlike particles; (iii) a geometrical approximation to obtain the orientational dependence of the interactions.

To effect (i) above, we implement the mean-field theoretic approach detailed in ref 6 for a system consisting of flat surfaces immersed in a polymer solution. The polymer is modeled as Gaussian chains with the solvent-mediated excluded-volume interactions between the monomers accounted in terms of an excluded-volume parameter denoted as $\upsilon$. The specific interactions between the polymer segments and the surface of particles are expressed in terms of inverse adsorption length $\lambda'$, which can be mapped onto a square well interaction potential between the polymer and the particle.[47] Explicitly, if the range of the square well potential is denoted as $\delta$ and its depth as $u_0$, then

$$\lambda' = \pi^2(u_0 - u_c)/8u_c\delta \tag{1}$$

where $u_0$ represents the change in the free energy of the system (all energies are expressed in $k_BT$ units) when a polymer segment adsorbs on the surface of particle, replacing solvent molecules, and can be experimentally measured by the chromatographic method.[48] $u_c$ is termed as the critical interaction strength and is related to the polymer segment length $b$ as $u_c = \pi^2b^2/24\delta^2$. Physically, $u_c$ represents the interaction strength characterizing the transition between a "depleting" to an "adsorbing" polymer.[49] Explicitly, a positive $\lambda'$ ($u_0 > u_c$) represents the case of adsorbing polymer where there is an enhanced polymer density at the surface of the particle, whereas a negative $\lambda'$ ($u_0 < u_c$) corresponds to the case of polymer depletion where there is a

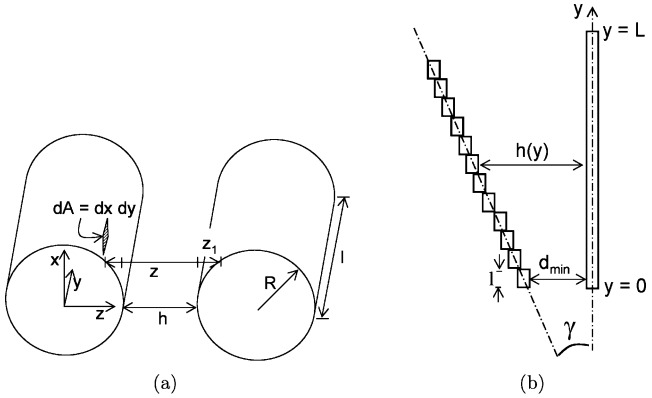


**Figure 1.** (a) Geometry for Derjaguin integration for parallelly oriented cylinders. (b) Geometrical construction for Derjaguin approximation for rods oriented at an angle $\gamma$ to each other.

reduced density at the surface. In experimental systems, $\lambda'$ can be characterized through neutron scattering measurements.[50] Most nanofillers are also typically characterized by a finite adsorption capacity which is accounted in our model as an additional entropic cost manifesting when the concentration of adsorbed polymer at the surface approaches a specified surface saturation concentration denoted as $\phi_m$.[6]

The McMillan−Mayer framework[51] is used to map the two-component system of polymers and particles onto a one-component system by integrating out the polymer degrees of freedom. This approach allows one to deduce the polymer mediated effective interactions between the flat surfaces in terms of the grand canonical partition functions of the polymer component with appropriate boundary conditions.[6,52] The latter are computed by implementing polymer self-consistent-field theory in a 1-D Cartesian coordinate system. Since the implementation details of this step are identical to that detailed in refs 6 and 44, we refrain from elaborating on them here.

To effect (ii), we use the above-derived "effective" interaction potentials within a Derjaguin approximation to evaluate the interaction potential between two rods in parallel configuration. Consider two parallelly oriented cylindrical rods with radius $R$ and length $l$ at a distance $h$ apart as shown in Figure 1a. The interaction potential between a differential surface element d$A$ (= d$x$ d$y$) on the first surface and a similar differential element on the second cylinder surface can be written as $E_{fp}(z)$ d$x$ d$y$, where $z \approx h + x^2/R$ and $E_{fp}(z)$ denotes the effective interaction per unit surface area between two flat surfaces at a distance $z$ apart. The total interaction energy can then be expressed as

$$E_{||}(h) = l\sqrt{R}\int_h^{h+2R} \frac{E_{fp}(z)}{\sqrt{z-h}}\,dz \tag{2}$$

To identify the *orientation dependence* of the interaction potentials (step iii), we use a geometrical construct shown schematically in Figure 1b. We assume one of the rods to be fixed at the origin along the $y$ axis and represent the other rod inclined at an angle $\gamma$ with respect to the first rod as a series of subsegments each parallel to the axis of the first rod and arranged along the orientation angle $\gamma$. The local inter-rod distance $h(y,\gamma)$ can be expressed in terms of the minimum distance between the rods $d_{min}$ as

$$h(y,\gamma) = d_{min} + y\tan\gamma \tag{3}$$

The orientation dependent interaction $E_{orient}(L,d_{min},\gamma)$ is then approximated as a sum of the interactions of all parallel subsegments as

$$E_{orient}(L,d_{min},\gamma) = \sum_{y=0}^{L} E_{||}[h(y,\gamma)] \tag{4}$$

Averaging over all translational configurations yields the average orientation-dependent interaction potential between two rods of length $L$ as

$$\bar{E}_{orient}(L,d_{min},\gamma) = \frac{1}{2}L\int_{-L}^{L} E_{orient}(L'(y'),d'_{min}(y'),\gamma)\,dy' \tag{5}$$

where $L'(y')$ is the length of overlap between two rods when one of the rods is displaced by a distance $y'$ along the $y$ axis and is given by $L - |y'|$, while the minimum distance between the rods $d'_{min}(y')$ can be obtained as

$$d'_{min}(y') = \begin{cases} d_{min} & \text{if } y' \le 0 \\ d_{min} + y'\tan\gamma & \text{if } y' > 0 \end{cases}$$

The orientation-dependent second virial coefficient $B_2(\gamma)$ is then obtained as[53]

$$B_2(\gamma) = \int_{2R}^{\infty} (\exp^{-\bar{E}_{orient}(L,d_{min},\gamma)} - 1)\, r^2\,dr; \quad r = 2R + d_{min} \tag{6}$$

**B. Phase Behavior: Flory Theory for Anisotropic Interactions.** We extend the Flory theory for isotropic−nematic phase transition[12] to include the above-derived polymer-mediated effective interactions. For this, we first expand the orientation dependent second virial coefficient $B_2(\gamma)$ (eq 6) in terms of Legendre polynomials

$$B_2(\gamma) = \sum_{n\ge 0} C_{2n} P_{2n}(\cos\gamma) \tag{7}$$

where $P_{2n}$ denotes the Legendre polynomial of order $2n$. Note that by the symmetry considerations only the even coefficients $C_{2n}$ are nonzero. The angle $\gamma$ between the cylindrical axes of two rods is related to the respective angles $\theta_1$ and $\theta_2$ between these axes and the space-fixed axis, and the respective azimuthal angles $\phi_1$ and $\phi_2$ as

$$\cos\gamma = \sin\theta_1\sin\theta_2\cos(\phi_1 - \phi_2) + \cos\theta_1\cos\theta_2 \tag{8}$$

Fixing the orientation of rod 1 and averaging over the orientation of rod 2 enables one to write

$$\langle P_{2n}(\cos\gamma)\rangle = P_{2n}(\cos\theta_1)\langle P_{2n}(\cos\theta)\rangle \tag{9}$$

where $\langle ... \rangle$ denotes the average over the distribution of orientations. The subscript 2 is dropped on the assumption that the orientations $\theta_1$ and $\theta_2$ are uncorrelated. Substituting eq 9 in eq 7, the orientation-dependent polymer-induced interaction that a rod segment (oriented at an angle $\theta_1$ with the fixed axis) experiences can be written as

$$\epsilon(\theta_1) = \sum_{n\ge 0} C_{2n} P_{2n}(\cos\theta_1)\langle P_{2n}(\cos\theta)\rangle \tag{10}$$

The subscript 1 can be omitted if the $\epsilon(\theta_1)$ is interpreted as the *mean* polymer-induced interaction for a rod segment. The total orientation-dependent contribution to the free energy for the system is then obtained by summing over all $an_xv_x/2$ pairs of rod segments as

$$H_{orient}(\theta) = -\frac{an_xv_x}{2}\sum_{n\ge 0} C_{2n} P_{2n}(\cos\theta)\langle P_{2n}(\cos\theta)\rangle \tag{11}$$

where $a$ is the aspect ratio of the rods, defined as $a = L/2R$; $\upsilon_x$ is the volume fraction of rods, defined as $an_x/(an_x + n_1)$ where $n_1$ and $n_x$ represent the number of solvent and solute (rod) molecules, respectively. The total free energy of the system can then be expressed as

$$H = n_1 \log(\upsilon_1) + n_x \log\left(\frac{\upsilon_x}{a}\right) - (n_1 + \bar{y}n_x) \log\left[1 - \upsilon_x\left(1 - \frac{\bar{y}}{a}\right)\right] - n_x(\bar{y} - 1) - \sum_\theta n_{x\theta} \log\left(\frac{n_x}{n_{x\theta}} \sin\theta\right) + \sum_\theta H_{\text{orient}}(\theta) \quad (12)$$

where $n_{x\theta}$ represents the number of rods that assume orientation $\theta$ with respect to the preferred axis of orientation. The first four terms in eq 12 correspond to the entropic contributions arising from hard rod excluded-volume interactions whereas the fifth and sixth terms represent the orientational entropic contribution. These terms are identical to that in the original Flory theory for hard rods.[11,12] The last term in the eq 12 corresponds to the effective inter-rod interactions arising from the presence of and interactions with the polymer. The equilibrium orientation distribution function, $n_{x\theta}/n_x$, which minimizes the above free energy can be obtained as

$$\frac{n_{x\theta}}{n_x} = f_1^{-1} \sin\theta \exp[-\alpha \sin\theta - H_{\text{orient}}(\theta)] \quad (13)$$

where

$$f_1 = \int_0^{\pi/2} \sin\theta \exp[-\alpha \sin\theta - H_{\text{orient}}(\theta)]\, d\theta \quad (14)$$

and

$$\alpha = -\frac{4}{\pi} a \log[1 - \upsilon_x(1 - \bar{y}/a)] \quad (15)$$

with $\bar{y}$ representing physically the equilibrium disorder in the distribution of rods with respect to the preferred axis of orientation:

$$\bar{y} = \int_0^{\pi/2} \left(\frac{4}{\pi} a \sin\theta\right) \frac{n_{x\theta}}{n_x}\, d\theta \quad (16)$$

The averages $\langle P_{2n}(\cos\theta)\rangle$ can then be expressed in terms of the above distribution function as

$$\langle P_{2n}(\cos\theta)\rangle = f_1^{-1} \int_0^{\pi/2} P_{2n}(\cos\theta) \sin\theta \exp[-\alpha \sin\theta - H_{\text{orient}}(\theta)]\, d\theta \quad (17)$$

To determine the phase behavior of the system, we require the chemical potentials of the rods (denoted as $\mu_{x_{an}}$) and solvent (denoted as $\mu_{1_{an}}$) components. For the anisotropic phase, these are obtained from eq 12 as

$$\mu_{x_{an}} = \frac{\partial H}{\partial n_x} = \log(\upsilon_x/af_1) + \upsilon_x(\bar{y} - 1) + a\upsilon_x^2/2 \sum_{n\geq 0} C_{2n} \langle P_{2n}(\cos\theta)\rangle^2 \quad (18a)$$

and

$$\mu_{1_{an}} = \frac{\partial H}{\partial n_1} = \log(\upsilon_1) - \log\left[1 - \upsilon_x\left(1 - \frac{\bar{y}}{a}\right)\right] + \upsilon_x^2/2 \sum_{n\geq 0} C_{2n} \langle P_{2n}(\cos\theta)\rangle^2 \quad (18b)$$

For the isotropic phase, $f_1 = 1.0$, $\bar{y} = a$, and $P_{2n} = 0$ for $n \geq 1$, and the chemical potentials can be identified as

$$\mu_{x_i} = \log(\upsilon_{x_i}/a) + \upsilon_{x_i}(a - 1) + a\upsilon_{x_i}^2 C_0/2 \quad (19a)$$

and

$$\mu_{1_i} = \log(\upsilon_{1_i}) + \upsilon_{x_i}^2 C_0/2 \quad (19b)$$

The volume fractions in the coexisting phases are then obtained by equating chemical potentials for individual components (solvent and rod) in the different phases and by a numerical solution of the resulting equations. It should be noted that we implement a semigrand canonical formalism (canonical for the particles and grand canonical for the polymer)[54] to compute the pair potentials within the McMillan−Mayer framework.[6,44] Thus, equilibrium of the polymer component between the different phases is automatically ensured by using the pair potentials computed at a fixed activity coefficient of polymer. Characterization of the anisotropic phase in terms of the equilibrium disorder parameter $\bar{y}$ requires the simultaneous solution of eqs 14, 16, and 17 for a fixed volume fraction of rods, which is then utilized to determine the phase coexistence from eqs 18 and 19. To effect the solution of above equations, we truncate the expansion of second virial coefficient $B_2(\gamma)$ (cf. eq 7) at $n = 10$, which was found to lead to an excellent convergence of the volume fractions of rods in coexisting phases (for hard rods, $n = 3$ was found to be sufficient for accurate results[55]). We note that the order parameters predicted in our model (not displayed in the results) at the onset of the I−N transition are quite high, $\langle P_2\rangle > 0.9$, suggesting a strongly first-order transition. The values of the order parameters are, however, consistent with the Flory predictions for hard rods of similar aspect ratios.

**C. Percolation Thresholds.** To analyze the onset of percolation of the rods, we use a simple connectivity criterion. We construct a "phantom" shell of thickness $\delta$ around the impenetrable rod[56] and define the connectivity between the rods in terms of the overlap probabilities of shells of thickness $\delta$ for different rods.[57] Physically, the shell thickness $\delta$ can be envisioned as the range over which an external perturbation (such as stress, electron transport) gets transferred from a particle to another. In many previous instances,[57,58] a "permeable" particle model has been used to delineate percolation threholds. However, for rodlike particles such as carbon nanotubes and nanofibers, the particles are expected to have a hard core, and hence the "core−shell" model of connectivity is expected to be more appropriate than the permeable rod models of percolation. Moreover, such an approach also corresponds to the methodology typically used in the computer simulations to deduce connectivity percolation.[59,60]

Warren[21] has derived an analytical expression for overlap volume $\upsilon_{ov}$ between shells enclosing long rodlike particles. Using his result (cf. eq A1, Appendix in ref 21), we express the probability of intersection between two rods as

$$\bar{P} \propto V_{ov}/V \approx \frac{2L^2 \sin\gamma}{V} \int_{2R}^{2(R+\delta)} \frac{f(z)}{\sin\gamma}\, g(z)\, dz \quad (20)$$

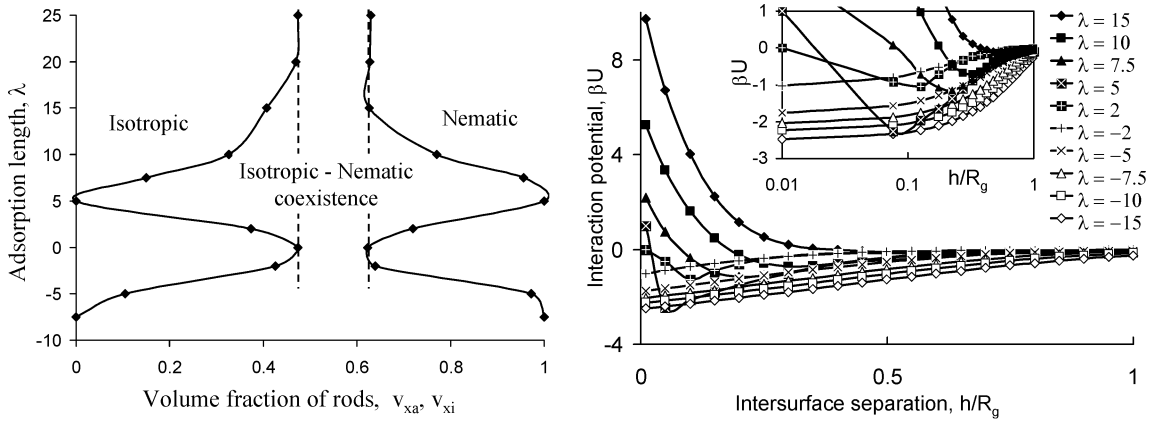


**Figure 2.** (a) Phase diagram in inverse adsorption length $\lambda$ vs volume fraction of rods plane for $R = 0.25R_g$, $L/D = 15$, and $\phi = 2.58$. The dotted lines show the phase diagram for hard rods with the same aspect ratio. (b) Pair interaction potential $\beta U$ as a function of intersurface distance (normalized by $R_g$) $h/R_g$ for polymer concentration $\phi = 2.58$ and $\lambda = \pm 15$, $\pm 10$, $\pm 7.5$, $\pm 5$, and $\pm 2$. The inset displays the attractive part of the interaction potentials on a semilog scale.

where $V$ denotes the volume of the system and $f(z)/\sin\gamma$ represents the overlap shell volume for two infinitely long cylinders oriented at angle ($\gamma$) with each other and a distance $z$ apart. The latter can be expressed as

$$\frac{f(z)}{\sin\gamma} = \frac{1}{\sin\gamma}\int_{-(R+\delta)+z/2}^{(R+\delta)-z/2} 4[(R+\delta)^2 - (z/2+p)^2]^{1/2}[(R+\delta)^2 - (z/2-p)^2]^{1/2}\,dp \quad (21)$$

In the above, $g(z)$ represents the radial distribution function for the rods, for which we use its low density approximation[61] as $g(z) = (1/2\pi)\int_0^{2\pi}\exp[-\beta\bar{E}_{orient}(L,z,\gamma)]\,d\gamma$ with $\beta\bar{E}_{orient}(L,z,\gamma)$ denoting the polymer-induced effective interaction potential between the two rods (cf. eq 5).

For a finite volume fraction $v_x$ of particles, the probability of intersection of a rod with at least $i$ other rods can be expressed in terms of $\bar{P}$ as[62]

$$P_{i,N} = 1 - \sum_{k=0}^{i-1}\binom{N}{k}\bar{P}^k(1-\bar{P})^{N-k} \quad (22)$$

where $N$ is the total number of rods in the volume $V$. From eq 22, we obtain the probability of a rod being connected with at least two rods as

$$P_{2,N} = 1 - (1-\bar{P})^N - N\bar{P}(1-\bar{P})^{N-1} \approx 1 - \exp\left[\frac{-v_x V_{ov}}{\pi R^2 L}\right]\left(1 + \frac{v_x V_{ov}}{\pi R^2 L}\right) \quad (23)$$

The percolation threshold $v_{perc}$ is then (somewhat arbitrarily) assigned as the volume fraction of rods at which $P_{2,N} = 0.5$, equivalent to the situation of sufficient likelihood for a rod being connected to at least two other rods.

**D. Parameters.** Our objective in this work is to study the role of parameters such as polymer−particle interaction strengths and polymer concentrations upon the stability and equilibrium phases of rodlike particles. We have studied two particle-to-polymer size ratios of $R/R_g = 0.25$ and 0.5, both of which fall in the "nanoparticle" regime where radius of particle is comparable to/or smaller than the radius of gyration of the polymer. We have varied the aspect ratio of rods from $a = L/2R = L/D = 15$ to 100 and limit ourselves to identification of the isotropic and nematic phases in such systems. We primarily consider polymer concentrations falling in the semidilute regimes and under "good solvent" conditions. Correspondingly, the non-dimensional excluded-volume parameter $B = \upsilon N^2/R_g{}^d$ is chosen to be 10. In the following, all polymer concentrations are normalized by the overlap concentration, $\rho^*$ as $\phi = \rho/\rho^*$, and our results correspond to $\phi > 1.0$ (indicating the semidilute concentration regime). In this article, the normalized inverse adsorption length $\lambda = \lambda' N/R_g$ is varied from $\lambda = -15$ to 25. These adsorption strength values span the situations of very low to high affinity between polymer segments and the particle surface (cf. eq 1). The surface capacity for adsorption is fixed by setting the surface saturation concentration $\phi_m$ to 20. In determining the percolation thresholds, the thickness of overlap shell for the particles (cf. eq 20) is assumed to be $\delta = 0.4R$. We briefly discuss the implications of this choice later.

## III. Phase Behavior of Hard Rods in the Presence of Polymer

In this section, we present results for the interactions and phase behavior of hard rods in polymer solutions and discuss the effects of different physical parameters such as adsorption strengths, polymer concentrations, radius of rods, and aspect ratios of rods.

**A. Effect of Adsorption Length $\lambda$.** In Figure 2a, we present the "phase diagram" (in the plane of adsorption length $\lambda$ vs rod volume fraction) for a dispersion of monodisperse rods of radius $R = 0.25R_g$ and aspect ratio $L/D = 15$ in a polymer solution of concentration $\phi = 1.29$. The dotted lines represent the corresponding coexistence volume fractions for a solution of hard rods (i.e., in the absence of polymer) with the identical aspect ratio. It is seen that the addition of interacting polymers significantly affects the topology of the phase diagram. Addition of nonadsorbing/weakly adsorbing polymer ($\lambda < 0$) leads to a distinct widening of the coexistence region which shifts the isotropic−nematic transitions to very dilute particle volume fractions. With an increase in the polymer−particle adsorption strength, we observe a narrowing of the coexistence region which leads to a decrease in the volume fraction of the nematic phase and an increase in the volume fraction of isotropic phase. $\lambda = 0$ (corresponding to $u_0 = u_c$, cf. eq 1) represents the condition of critical adsorption strength,[63] for which the effective rod−rod interactions are identical to that of original hard rod mixture. Consequently, the coexistence volume fractions equal that for a dispersion of hard rods of the same aspect ratio. For

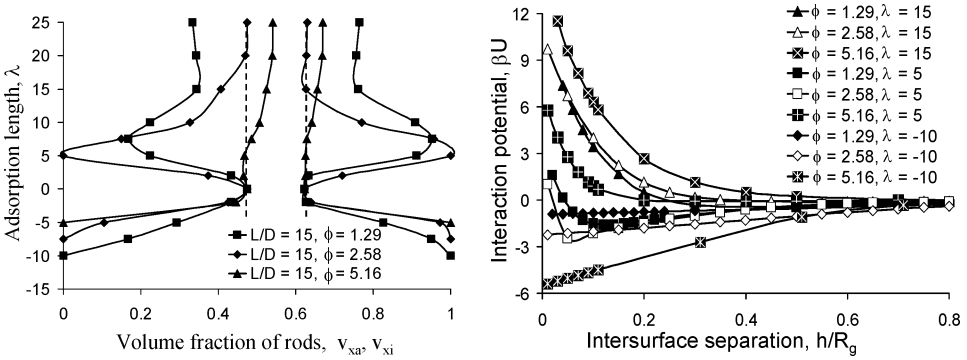


**Figure 3.** (a) Phase diagram in inverse adsorption length $\lambda$ vs volume fraction of rods plane for $R = 0.25R_g$, $L/D = 15$, and $\phi = 1$, 29, 2.58, and 5.16. The dotted lines show the phase diagram for hard rods with same aspect ratio. (b) Pair interaction potential $\beta U$ as a function of intersurface distance (normalized by $R_g$) $h/R_g$ for polymer concentrations $\phi = 1.29$, 2.58, and 5.16 and $\lambda = 15$, 5, and $-10$.

stronger adsorbing polymers ($\lambda > 0$), we observe first a widening of phase coexistence region, leading to a complete immiscibility of the rods at moderate adsorption strengths. However, further increase in adsorption strength is seen to result in a gradual narrowing of the demixed region and a stabilization of rods at higher adsorption strengths. At the highest adsorption strengths, the coexistence volume fractions are observed to correspond to that for the hard rods.

The above trends in the phase diagram can be rationalized on the basis of the effect of $\lambda$ on the effective interaction between surfaces. In Figure 2b, we display the polymer-induced effective interaction potentials $\beta U$ ($\beta = 1/k_BT$) as a function of intersurface separation $h/R_g$. The inset depicts the attractive part of the interaction potentials on a magnified, semilogarithmic scale. For the case of depleting polymers ($\lambda < 0$), the interactions are seen to be purely attractive, with an increase in the attraction strength as the intersurface distance is decreased. It is also evident from the inset to Figure 2b that an increase in $\lambda$ leads to a corresponding decrease in the strength of attractive interactions. These trends can be understood by noting that, for the case of negative $\lambda$, the polymer is depleted from the vicinity of the surface; the resultant osmotic imbalance for the polymer induces an effective attraction between the surfaces. With an increase in the $\lambda$, the depletion effect and correspondingly the entropic loss for the polymer diminish, resulting in a weakening of the induced attractions. The result is, at low (negative) $\lambda$ values, the strong depletion-induced effective attraction between the rods results in a highly negative second virial coefficient, and hence, the rods are nearly insoluble and we observe a wide region of immiscibility at low values of $\lambda$. On the other hand, with an increase in the adsorption strength, the weakening of depletion-induced attractions results in the narrowing of the two-phase region.

The presence of a stronger adsorbing polymer ($\lambda > 0$) is seen to result in nontrivial interaction potentials. Generically, the adsorbing polymer is observed to induce repulsive interactions at shorter distances followed by an attractive minimum at larger separations between the surfaces. With an increase in the $\lambda$ values, the strength of short distance repulsion is observed to increase, while the depth of attractive minimum first increases from zero at $\lambda = 0$ to a maximum value followed by a decrease at higher $\lambda$ values. As detailed in the ref 6, the intersurface interactions in presence of adsorbing polymers are governed by an interplay among three factors: (i) The polymer attempts to increase the number of surface contacts by forming bridges between the surfaces, thus resulting in an enthalpic gain. (ii) Upon confinement, the adsorbed polymer experiences an entropic cost arising from the monomeric excluded-volume interactions. (iii) As the surface concentration of adsorbed polymer approaches the maximum adsorption capacity of the surface, the entropic cost arising from the surface saturation constraint starts to manifest. At large intersurface distances, entropic repulsions arising from both the confinement and the surface saturation are negligible, and the resulting intersurface interactions are due to the enthalpic gain arising due to the adsorption. With a decrease in the intersurface distance, the confinement and the surface saturation entropy costs become comparable to enthalpic gain, resulting in the minimum manifested in the interaction potentials. At even smaller distances, the confinement and saturation entropy losses dominate the enthalpic gain arising from bridging rendering the intersurface interactions repulsive. For small but positive values of $\lambda$, the polymer adsorption is weak, and thus the enthalpic gain is also small, resulting in weak interactions. An increase in $\lambda$ facilitates adsorption of polymer, and the resulting enthalpic gain induces strong attractions at intermediate intersurface distances. For very high values of $\lambda$, the individual surfaces are saturated, and bringing them closer results in purely repulsive interactions between the surfaces. These nonmonotonic interactions for adsorbing polymers result in the observed phase topology where the two-phase region first widens, corresponding to increasing (bridging) attractions between the rods, and then with increase in $\lambda$ narrows down due to weakening of attractive interactions and strengthening of repulsions (steric stabilization).

Our results above suggest a novel "reentrant" phase behavior where at a fixed volume fraction of rods and polymers the dispersion is immiscible at weak interactions (depletion), then becomes stable and again immiscible as strength of polymer−particle interaction is increased, and then finally again stable for the highest attractions. We note that similar reentrant miscibility has been predicted for spherical particles by Hooper and Schweizer.[8] In a nutshell, our results suggest two optimal conditions for creating stable dispersions for a hard rod system: addition of either (i) weakly adsorbing ($\lambda \simeq 0$) or (ii) extremely strongly adsorbing ($\lambda \gg 0$) polymers. These results may have implications in choosing appropriate polymeric solvent for stabilization or separation of rodlike particles.

**B. Effect of Polymer Concentration.** In Figure 3a, we display the effect of the polymer solution concentration on the phase behavioral characteristics. For nonadsorbing/weakly adsorbing polymers ($\lambda < 0$), the phase diagrams are seen to follow a qualitatively similar behavior for all concentrations, with a monotonic expansion of the coexistence region with an increase in the polymer concentrations for such systems. As evident from Figure 3b, which displays the pair interaction potentials $\beta U$ as a function of intersurface distance $h/R_g$ for different polymer concentrations, the strength of depletion attraction increases with

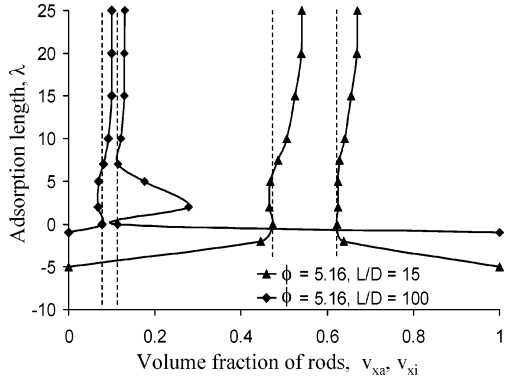


**Figure 4.** Phase diagram in inverse adsorption length $\lambda$ vs volume fraction of rods plane for $R = 0.25R_g$, $\phi = 5.16$, and $L/D = 15$ and 100. The dashed lines show the phase diagram for hard rods with the same aspect ratios.

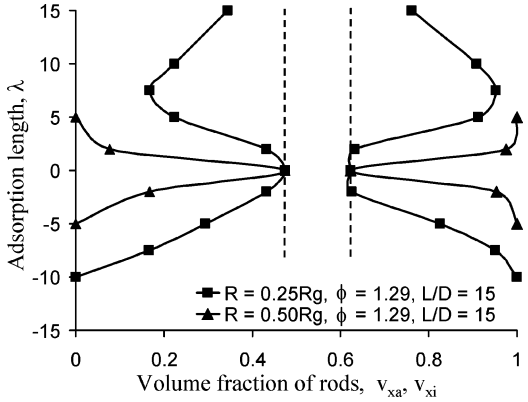


**Figure 5.** Phase diagram in inverse adsorption length $\lambda$ vs volume fraction of rods plane for $R = 0.25R_g$, $\phi = 1.29$, and $L/D = 15$. The dotted lines show the corresponding phase diagram for hard rods with the same aspect ratio.

an increase in the concentration of polymers which rationalizes this widening of the region of coexistence.

In contrast, for the case of stronger adsorbing polymers ($\lambda > 0$), the phase topology reflects a sensitive interplay between the polymer concentrations and the adsorption strength. For small positive $\lambda$, we observe that with an increase in $\phi$, the region of immiscibility first widens and then shrinks to isotropic−nematic coexistence similar to hard rod behavior at higher $\phi$ values. The above trends can be explained by the fact that for moderate adsorption strengths an increase in the polymer concentration initially leads to an increase in the bridging, rendering the induced effective interactions strongly attractive (cf. Figure 3b). This leads to a wider region of immiscibility. However, further increase in polymer concentrations results in a saturation of the surfaces and an increase in the confinement-induced entropic costs, resulting in both a strengthening of the short-distance repulsions and a weakening of the attractions. This leads to a narrowing of the coexistence regions. At higher $\lambda$ values, the entropic repulsions dominate, resulting in a narrowing of two-phase region monotonically with increase in the polymer concentrations. For the highest $\phi$ values, the purely repulsive interactions lead to a phase behavior which resembles that of the hard rods and corresponds physically to the phase coexistence of polymer-coated rods.

**C. Effect of Aspect Ratio.** In Figure 4, we display the effect of the aspect ratio of rods on the phase diagrams. The radius of the rods is fixed at $R = 0.25R_g$, and the polymer concentration is $\phi = 5.16$. The dotted lines represent corresponding coexistence curves for hard rods with the same aspect ratios. For longer rods, we observe that addition of depleting or weakly adsorbing polymers induces immiscibility at nearly all negative values of $\lambda$. This situation can be contrasted for shorter rods where stable regions were found for weakly depleting polymers. For the case of adsorbing polymer ($\lambda \geq 0$), an increase in the aspect ratio of rods is observed to shift the region of coexistence to much lower volume fractions. For larger rods, increase in the adsorption strength results in widening of coexistence region, followed by a narrowing to hard rod coexistence behavior at higher adsorption strengths. In contrast, the smaller rods are observed to follow a hard rod coexistence behavior at all positive adsorption strengths. At higher adsorption strengths, we observe that the coexistence volume fractions shift toward higher values for all aspect ratios.

The above differences in the phase behavior can be understood by noting that the strength of the interrod interactions is proportional to the length of the rods. For negative adsorption lengths, increasing the aspect ratio results in very strong depletion attractions, which induces stronger immiscibility for the case of longer rods. For moderate adsorption strengths, the polymer induced interactions are characterized by short distance repulsions followed by long distance attractions (cf. Figure 2b). An increase in the aspect ratio again results in strengthening of these interactions whose interplay results in a widening of the coexistence region. For higher adsorption strengths, the polymer induces purely repulsive interactions which rationalizes the observed trends as equivalent to the phase behavior of polymer-coated rods with renormalized radii determined by the strength of the repulsions.

**D. Influence of the Radius of Rods.** In Figure 5 we analyze the effect of the radius of the rods (relative to the size of the polymer which is assumed to be fixed) on the topology of the phase diagram for fixed aspect ratio $L/D = 15$ and polymer concentration $\phi = 1.29$. An increase in the radius of the rods is observed to result in a significant broadening of the two-phase region for both adsorbing and nonadsorbing polymers. The above effects are rationalized in terms of increase in the strength of attractive interactions with increase in the radius of the rods. In the case of depleting polymers $\lambda < 0$, increasing the rod size correspondingly increases the depleted volume for the polymer, making the inter-rod attractions stronger for thicker rods. Whereas for adsorbing polymers, the increase in the adsorbing surface area enhances polymer-induced bridging and correspondingly increases the depth of the inter-rod attractive minimum. Even at higher $\lambda$ values where the induced short distance repulsions are stronger, the strong long-range attractive interactions dominate the phase behavior, leading to complete insolubility of thicker rods.

## IV. Percolation Thresholds

In this section, we consider the percolation thresholds $v_{perc}$ (defined by eq 23) and their locations relative to the phase coexistence. Shown in Figure 6 are the lines of percolation thresholds in the adsorption strength vs volume fraction plane for hard rods (Figure 6a,b). The dashed lines in Figure 6 correspond to the phase coexistence curves for the same parameters. For the specific choice of overlap shell thickness $\delta$ we have adopted ($\delta = 0.4R$); we observe that the overall topology of the percolation lines follows the respective isotropic branch of the phase coexistence curves. This can be understood by noting that the onset of percolation corresponds physically to the point where the rods are connected and hence are also crowded and would rather order into a nematic phase. More interesting is the influence of polymers on the relative locations

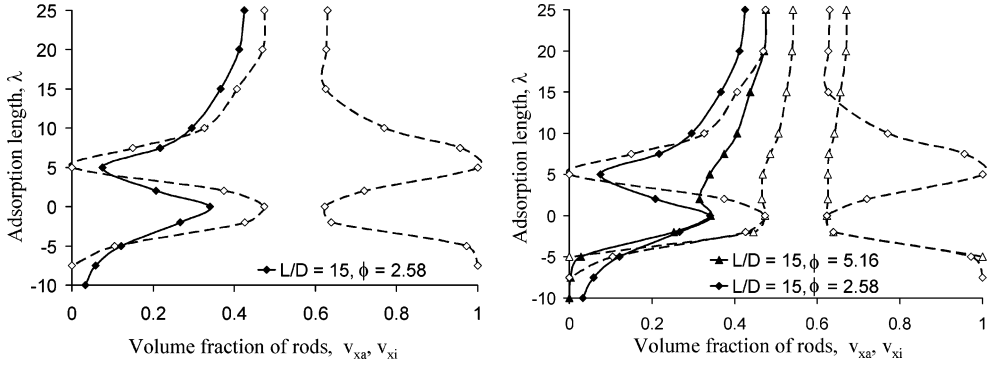


**Figure 6.** Percolation lines (solid lines) and phase coexistence curves (dashed lines) in inverse adsorption length $\lambda$ vs volume fraction of rods plane for $R = 0.25R_g$ for (a) hard rods with $L/D = 15$ and polymer concentration $\phi = 2.58$. (b) Hard rods with $L/D = 15$ and polymer concentration $\phi = 2.58$ and 5.16.

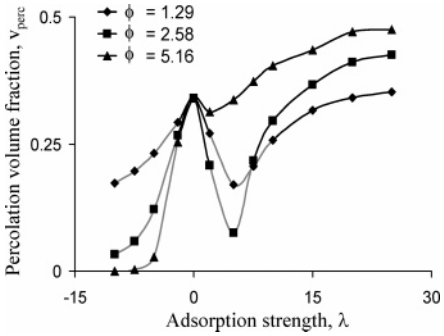


**Figure 7.** Percolation thresholds plotted as a function of inverse adsorption strength $\lambda$, for hard rods with $R = 0.25R_g$ for different polymer concentrations. The dark lines correspond to the stable isotropic dispersions, and light lines show the two-phase region.

of the percolation lines and the coexistence curves. For cases where the polymer-mediated interactions are strongly attractive, phase coexistence is predicted to preempt the percolation. Such situations occur in the context of strongly depleting polymers ($\lambda \ll 0$) and/ polymers with moderate attractive interactions with the particles ($\lambda > 0$, but $\lambda$ is not too large) (Figure 6a). Furthermore, at a given $\lambda$, lower polymer concentration is seen to promote the tendency to aggregate (Figure 6b). In such cases, while the attractive interactions bring the particles together (and hence promote percolation, as evident in the shift of percolation lines to lower volume fractions), the tendency to aggregate overwhelms the percolation characteristics (Figure 6b). In contrast, for cases where the interactions are weakly attractive and/or repulsive the percolation lines fall outside the phase coexistence lines. Such conditions result for weakly ($\lambda \gtrsim 0$ but small) and strongly adsorbing ($\lambda \gg 0$) polymers for hard rods. Moreover, at a given $\lambda$, higher polymer concentrations are seen to promote such a behavior.

Figure 7 summarizes the effect of polymer concentration on the stability and percolation thresholds for hard rods. The dark lines correspond to stable isotropic regions whereas light lines indicate that the percolation falls within the two-phase coexistence region. For the case of hard rods, it is seen that the addition of polymers with weakly depletion tendency or weakly adsorbing characteristics can be used to lower the percolation thresholds and still maintain the volume fraction in the stable isotropic region. However, addition of strongly adsorbing polymer results in a significant increase in the percolation thresholds. Hence, weakly depleting or weakly adsorbing polymers appear to be an optimal choice to promote percolation.

In many instances, the percolation thresholds have been shown to have a strong relationships with the aspect ratio of the rods, and simple linear scaling has been proposed to relate the thresholds to the particle anisotropy.[64] In Figure 8, we analyze whether such dependences also hold when the polymer-mediated interactions are included. In Figure 8a we display the percolation thresholds for the cases where percolation of rods occurs in the stable isotropic region. Incredibly, in almost all cases, we observe that the linear dependence of $v_{perc}$ on the inverse aspect ratio of rods still holds with, however, a slope which depends on the adsorption strength and bare interactions. The slope of such fits (displayed in Figure 8b) exhibits trends consistent with our above discussions. Explicitly, both weakly depleting and weakly adsorbing polymers lower the slopes and can decrease the percolation thresholds compared to that observed for hard rods. On the other hand, moderate and strong attractions increase the slopes and the corresponding percolation thresholds.

We note that the above predictions are by and large consistent with recent observations reported in the context carbon nanotubes[39] where an introduction of a weak depletion attraction was shown to decrease the percolation thresholds significantly. It should however be noted that our above analysis of percolation transitions does depend on the choice of connectivity shell thickness $\delta$. Broadly speaking, a lower (higher) value of $\delta$ shifts the percolation lines to higher (lower) volume fractions of rodlike particles. However, the qualitative effects arising from varying the strength of adsorption of polymers, the polymer concentrations, and aspect ratio of rods are still expected to remain similar to that portrayed in Figures 6−8. The implications of these findings on the optimal conditions for stable and percolated dispersions of rods will be discussed in more detail in section VI.

## V. Influence of van der Waals Attractions

As discussed in the Introduction, many nanoscale filler particles used in applications exhibit a strong tendency to aggregate due to strong interparticle van der Waals interactions.[33,65,66] While the previous sections focused on the case of rods with just hard body interactions, in this section we analyze the effect of polymers on the overall interactions and discuss the stability behavior of rodlike particles characterized by strong van der Waals attractions. For illustrative purposes, we have assumed a van der Waals interaction similar to that reported for the single wall nanotubes[33] with a depth of attraction of $\sim -40k_BT$/nm (cf. Figure 9 of ref 33). Within this framework, Figure 9a displays the resulting overall interactions (obtained by summing the van der Waals attraction and polymer-mediated effective interactions) between rodlike particles with aspect ratio

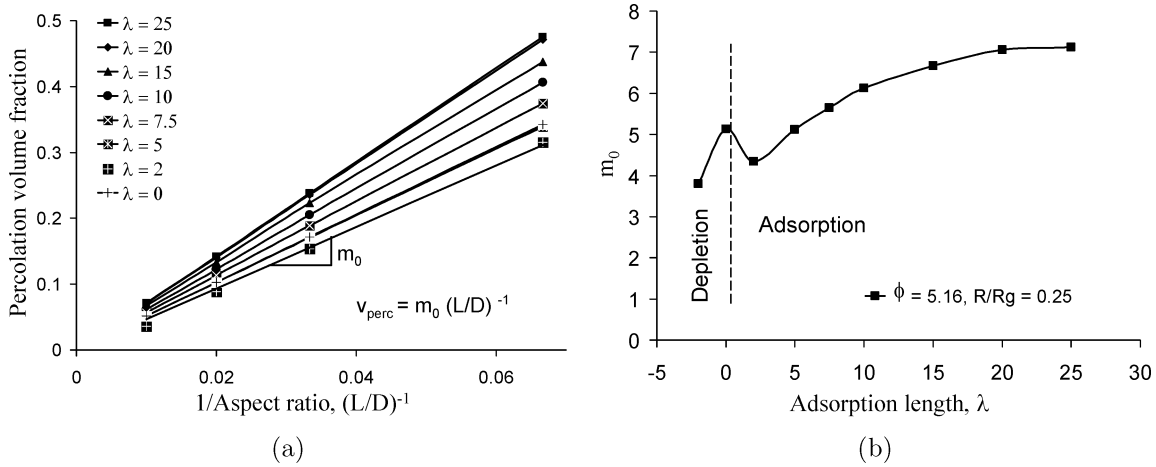


**Figure 8.** (a) Percolation thresholds $\upsilon_{perc}$ plotted as a function of inverse aspect ratio $(L/D)^{-1}$, for hard rods with $R = 0.25R_g$ and $\phi = 5.16$ for different adsorption strengths. (b) Slope $m_0$ of linear fits for percolation thresholds ($\upsilon_x = m_0(L/D)$) plotted as a function of $\lambda$ for hard rods.

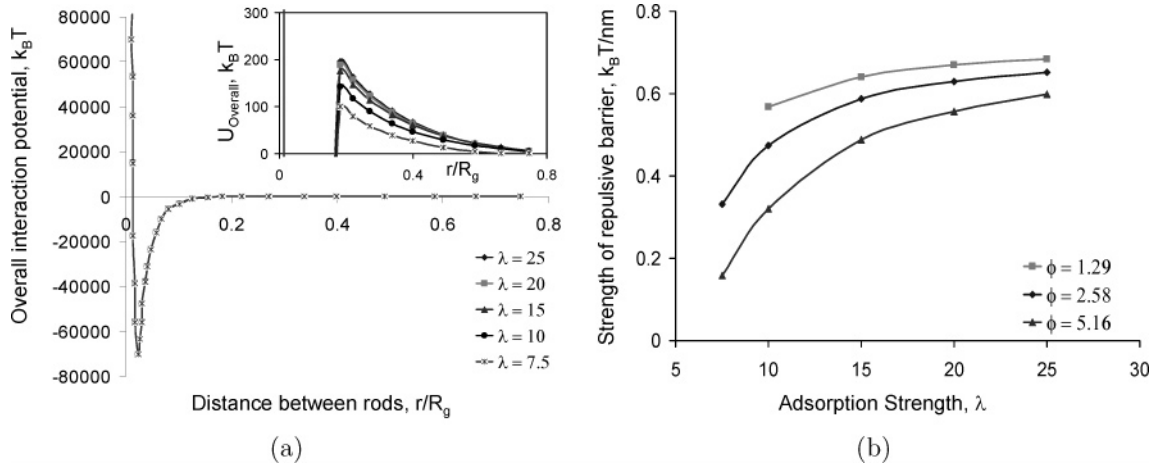


**Figure 9.** (a) Overall interactions between two parallel rods $\beta U$ as a function of inter-rod separation, $r/R_g$, for rods with $R = 1.5$ nm, $R_g = 6$ nm, and $L/D = 100$. The overall interactions are obtained as sum of the van der Waals interactions and the polymer-induced "effective" interactions ($\phi = 2.58$, $\phi_m = 15.0$). The inset shows polymer-induced long-range repulsive barrier in the overall interactions. (b) The strength of polymer induced repulsive barrier (in $k_BT$/nm units) as a function of adsorption strength for $R = 1.5$ nm, $R_g = 6$ nm, and polymer concentrations as indicated in the legend.

$L/D = 100$, $R = 1.5$ nm, and $R_g = 6$ nm. The inset magnifies the repulsive barrier introduced by the presence of polymer in the system. It is seen that at larger intersurface distances the polymer-induced long-range repulsions dominate the overall interactions, whereas at small intersurface distances the van der Waals attractions dominate. The main effect resulting from addition of a strongly adsorbing polymer is seen to be the occurrence of a significant repulsive barrier in the overall interactions, with the strength of repulsions increasing with an increase in $\lambda$. We note that the strength of the repulsive barrier depends on both the strength of adsorption and the concentration of polymer, as displayed in Figure 9b. The strength of repulsions shows a monotonic increase with increase in the adsorption strength at a fixed concentration of polymer and is observed to decrease with increase in the polymer concentration for a fixed adsorption strength. These observations can be rationalized in the manner similar to our earlier discussions on the influence of polymer concentration and adsorption strength on the polymer-induced repulsions.

The polymer-induced long-ranged repulsive barrier in the overall interactions can provide a kinetic stabilizing effect against the short-range van der Waals attractions in the dispersions of nanotubes. For equilibrium considerations, the presence of a weak long-range repulsive barrier (in comparison with the van der Waals attractions) can be expected to favor formation and stabilization of large equilibrium clusters on nanotubes, while preventing macrophase separation in the system. Formation of such equilibrium clusters under influence of weak long-range repulsions has been predicted for colloidal systems characterized by short-range attractive interactions.[67] In a future work, we plan to investigate the occurrence of such phases for rodlike particles.

## VI. Discussion

Our results suggest that the topology of the phase diagram of mixture of polymer and rods is highly dependent on the anisotropy of the rods, relative sizes of the rods and polymers, concentration of the polymer, and the strength of adsorption. For the case of nonadsorbing polymer, the polymer depletion-induced attractive interactions are found to result in a large two-phase region which widens with an increase in the polymer concentration. A number of previous theoretical[19] and experimental studies[68] report a similar trend in the phase behavior of rodlike particles such as bohemite rods, tobacco mosaic virus, etc., in the presence of nonadsorbing polymers. Addition of adsorbing polymers is observed to lead to a richer phase behavior where at high polymer concentrations the polymer-induced repulsive interactions result in steric stabilization of the rodlike particles, and the isotropic−nematic transition closely resembles that for hard rods. This "stabilizing" behavior has

also been exploited in a number of experimental studies, where steric stabilization induced by physical adsorption of polymers such as Gum Arabic are efficiently utilized to obtain stable dispersions of nanotubes.[69−71]

An interesting outcome of this study is the "reentrant" behavior of the phase diagram with change in the adsorption strength. At lower adsorption strengths, the depletion-induced attractions widen the two-phase region, which narrows to hard rod isotropic−nematic transition as the adsorption strength becomes zero. At positive adsorption strength, for a certain range of polymer concentrations, a distinct broadening of the two-phase region is predicted which subsequently narrows to a hard rod transition at higher adsorption strengths. Thus, at certain volume fractions of rods, the system goes from (coexisting isotropic−nematic)−stable isotropic/nematic−(coexisting isotropic−nematic)−stable isotropic/nematic phases as the surface affinity of the polymers is modified.

We note that the topology of the phase diagrams for mixtures of polymer and rodlike particles is influenced not only by the aspect ratio (size anisotropy) of rods but also by the relative sizes of the rods and the polymeric component (cf. section IIID). The latter dependence arises from the polymer-induced interactions which are dependent on the sizes of both the polymer and the particles. These results may have implications in the context of purification/separation applications where adsorbing polymers are added to pristine nanotubes in order to achieve selective dispersions of individual nanotubes and to separate the individual nanotubes from carbonaceous impurities/bundles of tubes.[34] By adding appropriate quantities of polymer with favorable physical properties ($\lambda$, molecular weight, etc.), it might be possible to achieve conditions that will favor stability of individual nanorods while facilitating separation/aggregations of the impurities/bundles of rods.

This work also studied the effectiveness of adsorbing polymers in increasing dispersability of rods characterized by strong van der Waals interactions. It is observed that for the case of moderate to strongly adsorbing polymer the polymer induces long-range repulsions between nanotubes and can reduce the effect of short-range van der Waals attractions and can prevent aggregation of nanotubes. Such an approach has already been used in a number of experimental investigations where adsorption of polymers leads to exfoliation and stabilization of dispersions of the tubes.[69−71]

We also examined the percolation thresholds and their relative location to the isotropic−nematic transition for hard rods. Our results predict a large region of percolated stable isotropic phase of rods dispersed in solutions of weakly depleting or adsorbing polymers. For adsorbing polymers, an increase in the polymer concentration and/or adsorption strength is observed to enhance the stability of rods. However, increase in adsorption strength also shifts the percolation transition to higher volume fractions. Thus, concentrated solutions of weakly adsorbing polymers or weakly depleting polymers appear to be an optimal choice for maximizing the properties (such as elastic modulus, electrical conductivity which are dependent on achieving a stable percolated phase at low volume fractions of rods).

## VII. Conclusion

In this article, the effect of polymer adsorption strength, polymer concentration, the relative sizes of rods and polymer, and aspect ratio of rods on the isotropic−nematic phase separation and percolation transitions in dispersions of rodlike particles in polymer solutions are studied. Within the polymer field theoretic framework, the polymer-mediated "effective" interactions between rodlike particles are deduced. To the best of our knowledge, this work presents the first systematic study on the polymer-induced interactions between rodlike particles and their dependence on the orientation of rods and should serve as a first step toward understanding the origin of complex phase behavior of rod−polymer mixtures. The above-derived polymer-induced effective interactions are incorporated into an adaptation of the Flory theory for anisotropic interactions to investigate the effect of polymer on the phase behavior and percolation transitions of rods. Our study delimits the physical parameters that affect the solubility, phase diagrams, and percolation thresholds of rodlike particles in the presence of polymers and indicates under what conditions percolated stable dispersions (or easier separations) of rods may be achieved. Our study concludes that the change in the polymer concentration and strength of adsorption may provide an attractive means to tune the interactions between the rods and to prevent van der Waals-induced bundling of nanotubes. The latter may help experimentalists in devising experiments that will result in better dispersions of technologically important rodlike systems such as nanotubes, carbon fibers, fullerenes, etc.

It should be noted that our study considers equilibrium or reversible adsorption of polymer on the surface of the particles and thus is not concerned with the nonequilibrium aspects of the polymer adsorption/desorption process. Further, our framework is also inadequate to account for the kinetic gelation effects that are reported to be important at high volume fractions of rods or for the case of strong depletion attractions.[68,72] The latter has been speculated to occur during quenches inside the phase coexistence region, when the percolation lines also fall within the coexistence region.[73] While we cannot comment on these effects, the relative locations of the percolation lines and phase coexistence curves provide a guideline for the occurrence of such phenomena. Another limitation of the study concerns the accuracy of the Derjaguin approximation. The latter is accurate in the limit where the radii of the curved surfaces are significantly larger than the intersurface separation. For the case of polymer-induced interactions, the range of interactions is relatively large, and in the present study the inter-rod distances where the interactions become negligible are comparable to the radius of the rods. The latter introduces inaccuracies in the quantitative description of interaction potentials. However, the qualitative trends predicted in this work are expected to still be accurate.

**Acknowledgment.** This work was supported in part by a grant from Robert A. Welch Foundation and by National Science Foundation under Award NSF CTS-0347381. We gratefully acknowledge the allocation of computer time in Texas Advanced Computing Center.

## References and Notes

(1) Asakura, S.; Oosawa, F. *J. Polym. Sci.* **1958**, *33*, 471.
(2) Vrij, A. *Pure Appl. Chem.* **1976**, *33*, 183.
(3) Poon, W. C. K. *Science* **2004**, *304*, 830.
(4) Scheutjens, J. M. H. M.; Fleer, G. J. *J. Phys. Chem.* **1979**, *83*, 1619. Scheutjens, J. M. H. M.; Fleer, G. J. *J. Phys. Chem.* **1980**, *84*, 178.
(5) Rossi, G.; Pincus, P. A. *Europhys. Lett.* **1988**, *5*, 641.
(6) Surve, M.; Pryamitsyn, V.; Ganesan, V. *Langmuir* **2006**, *22*, 969.
(7) Johner, A.; Joanny, J. F.; Diez, Orrite, S.; Bonet-Avalos, J. *Europhys. Lett.* **2001**, *56*, 549.
(8) Hooper, J. B.; Schweizer, K. S. *Macromolecules*, in press.
(9) Singh, C.; Pickett, G. T.; Zhulina, E.; Balazs, A. C. *J. Phys. Chem. B* **1997**, *101*, 10614.
(10) Onsager, L. *Ann. N.Y. Acad. Sci.* **1949**, *51*, 627.
(11) Flory, P. J. *Proc. R. Soc. London A* **1955**, *234*, 73.
(12) Flory, P. J.; Ronca, G. *Mol. Cryst. Liq. Cryst.* **1979**, *54*, 289.
(13) Wee, E. L.; Miller, W. G. *J. Phys. Chem.* **1971**, *75*, 1446.

(14) Morgan, P. W. *Macromolecules* **1977**, *10*, 1381.
(15) Straley, J. P. *Mol. Cryst. Liq. Cryst.* **1977**, *22*, 233.
(16) Flory, P. J.; Irvine, P. A. *J. Chem. Soc., Faraday Trans. 1* **1984**, *84*, 1807.
(17) Flory, P. J.; Ronca, G. *Mol. Cryst. Liq. Cryst.* **1979**, *54*, 311.
(18) Warner, M.; Flory, P. J. *J. Chem. Phys.* **1980**, *73*, 6327.
(19) Lekkerkerker, H. N. W.; Stroobants, A. *II Nuovo Cimento* **1994**, *16D*, 949.
(20) Vroege, G. J.; Lekkerkerker, H. N. W. *Reg. Prog. Phys.* **1992**, *55*, 1241.
(21) Warren, P. B. *J. Phys. I* **1994**, *4*, 237.
(22) Savenko, S. V.; Dijkstra, M. *J. Chem. Phys.* **2006**, *124*, 234902.
(23) O'Connell, M. J.; Boul, P.; Ericson, L. M.; Huffman, C.; Wang, Y. H.; Haroz, E.; Kuper, C.; Tour, J.; Ausman, K. D.; Smalley, R. E. *Chem. Phys. Lett.* **2001**, *342*, 265.
(24) Moniruzzaman, M.; Winey, K. I. *Macromolecules*, in press.
(25) Baughman, R. H.; Zakhidov, A. A.; de Heer, W. A. *Science* **2002**, *297*, 787.
(26) Vigolo, B.; Penicaud, A.; Coulon, C.; Sauder, R.; Pailler, C.; Journet, P.; Bernier, P.; Poulin, P. *Science* **2000**, *290*, 1331.
(27) O'Connel, M. J.; Bachilo, S. M.; Huffman, C. B.; Moore, V. C.; Strano, M. S.; Haroz, E. H.; Rialon, K. L.; Boul, P. J.; Noon, W. H.; Kittrell, C.; Ma, J.; Hauge, R. H.; Weisman, R. B.; Smalley, R. E. *Science* **2002**, *297*, 593.
(28) Wang, H.; Zhou, W.; Ho, D. L.; Winey, K. I.; Fischer, J. E.; Glinka, C. J.; Hobbie, E. K. *Nano Lett.* **2004**, *4*, 1789.
(29) Chen, J.; Hamon, M. A.; Hu, H.; Chen, Y.; Rao, A. M.; Eklund, P. C.; Haddon, R. C. *Science* **1998**, *282*, 95.
(30) Boul, P. J.; Liu, J.; Mickelson, E. T.; Huffman, C. B.; Ericson, L. M.; Chiang, I. W.; Smith, K. A.; Colbert, D. T.; Hauge, R. H.; Margrave, J. L.; Smalley, R. E. *Chem. Phys. Lett.* **1999**, *310*, 367.
(31) Ausman, K. D.; Piner, R.; Lourie, O.; Ruoff, R. S.; Korobov, M. *J. Phys. Chem. B* **2000**, *104*, 8911, 14850.
(32) Shvartzman-Cohen, R.; Nativ-Roth, E.; et al. *J. Am. Chem. Soc.* **2004**, *126*.
(33) Szleifer, I.; Yerushalmi-Rozen, R. *Polymer* **2005**, *46*, 7803.
(34) Yudasaka, M.; Zhang, M.; Jabs, C.; Iijima, S. *Appl. Phys.* **2000**, *71*, 449.
(35) Dalton, A. B.; Blau, W. J.; et al. *Synth. Met.* **2001**, *121*, 1217.
(36) Zheng, M.; Jagota, A.; Semke, E. D.; et al. *Nat. Mater.* **2003**, *2*, 338.
(37) Baskaran, D.; Mays, J. W.; Bratcher, M. S. *Chem. Mater.* **2005**, *17*, 3389.
(38) Sandler, J. K. W.; Kirk, J. E.; Kinloch, I. A.; Shaffer, M. S. P.; Windle, A. H. *Polymer* **2003**, *44*, 5893.
(39) Vigolo, B.; Coulon, C.; Maugey, M.; Zakri, C.; Poulin, P. *Science* **2005**, *309*, 920.
(40) Du, F.; Scogna, R. C.; Zhou, W.; Brand, S.; Fischer, J. E.; Winey, K. I. *Macromolecules* **2004**, *37*, 9048.
(41) Du, F.; Fischer, J. E.; Winey, K. I. *Phys. Rev. B* **2005**, *72*, 121404.
(42) Kashiwagi, T.; Du, F.; Douglas, J. F.; Winey, K. I.; Harris, Jr., R. H.; Shields, J. R. *Nat. Mater.* **2005**, *4*, 928.
(43) Wang, X. L.; Chatterjee, A. P. *J. Chem. Phys.* **2003**, *118*, 10787.
(44) Surve, M.; Pryamitsyn, V.; Ganesan, V. *J. Chem. Phys.* **2005**, *122*, 154901.
(45) Derjaguin, B. V. *Kolloid Z.* **1934**, *69*, 155.
(46) White, L. R. *J. Colloid Interface Sci.* **1983**, *95*, 286.
(47) Gorbunov, A. A.; Skvortsov, A. M. *Adv. Colloid Interface Sci.* **1995**, *62*, 31.
(48) van der Beek, G. P.; Cohen Stuart, M. A.; Fleer, G. J.; Hofman, J. E. *Langmuir* **1989**, *5*, 1180.
(49) de Gennes, P. G. *Macromolecules* **1981**, *14*, 1637.
(50) Cabane, B.; Duplessix, R. *Colloids Surf.* **1985**, *13*, 19.
(51) McMillan, W. G., Jr.; Mayer, J. E. *J. Chem. Phys.* **1945**, *13*, 276.
(52) Bonet-Avalos, J.; Johner, A.; Joanny, J. F. *J. Chem. Phys.* **1994**, *101*, 9181. Bonet-Avalos, J.; Johner, A. *Faraday Discuss.* **1994**, *98*, 111.
(53) McQuarrie, D. A. *Statistical Mechanics*; University Science Books: Sausalito, CA, 2000.
(54) Dijkstra, M.; van Roij, R.; Evans, R. *Phys. Rev. E* **1999**, *5*, 5744.
(55) Lekkerkerker, H. N. W.; Coulon, Ph.; van der Hagen, R. *J. Chem. Phys.* **1984**, *7*, 3427.
(56) Bug, A. L. R.; Safran, S. A.; Webman, I. *Phys. Rev. Lett.* **1985**, *55*, 1896.
(57) Bug, A. L. R.; Safran, S. A.; Webman, I. *Phys. Rev. B* **1986**, *33*, 4716.
(58) Foygel, M.; Morris, R. D.; Anez, D.; French, S.; Sobolev, V. L. *Phys. Rev. B* **2005**, *71*, 104201.
(59) Bolhuis, P. G.; Stroobants, A.; Frenkel, D.; Lekkerkerker, H. N. W. *J. Chem. Phys.* **1997**, *107*, 1551.
(60) Grujicic, M.; Cao, G.; Roy, W. N. *J. Mater. Sci.* **2004**, *39*, 4441.
(61) Hansen, J. P.; McDonald, I. R. *The Theory of Simple Liquids*; Academic Press: New York, 1976.
(62) Munson-McGee, S. H. *Phys. Rev. B* **1991**, *43*, 3331.
(63) Fleer, G. J.; Cohen Stuart, M. A.; Scheutjens, J. M. H. M.; Cosgrove, T.; Vincent, B. *Polymers at Interfaces*; Chapman & Hall: London, 1993.
(64) Philipse, A. P. *Langmuir* **1996**, *12*, 1127.
(65) Girifalco, L. A.; Hodak, M.; Lee, R. S. *Phys. Rev. B* **2000**, *62*, 13104.
(66) Shvartzman-Cohen, R.; Levi-Kalisman, Y.; Nativ-Roth, E.; Yerushalmi-Rozen, R. *Langmuir* **2004**, *20*, 6085.
(67) Groenewold, J.; Kegel, W. K. *J. Phys. Chem. B* **2001**, *105*, 11702.
(68) van Bruggen, M. P. B.; Lekkerkerker, H. N. W. *Macromolecules* **2000**, *33*, 5532.
(69) Bandyopadhyaya, R.; Nativ-Roth, E.; Regev, O.; Yerushalmi-Rozen, R. *Nano Lett.* **2002**, *2*, 25.
(70) Star, A.; Fraser Stoddart, J.; Steuerman, D.; Diehl, M.; Boukai, A.; Wong, E. W.; Yang, X.; Chung, S-W.; Choi, H.; Heath, J. R. *Angew. Chem.* **2001**, *40*, 1721.
(71) Coleman, J. N.; Dalton, A. B.; Curran, S.; Rubio, A.; Davey, A. P.; Drury, A.; McCarthy, B.; Lahr, B.; Ajayan, P. M.; Roth, S.; Barklie, R. C.; Blau, W. J. *Nat. Mater.* **2000**, *12*, 213.
(72) van Bruggen, M. P. B.; van der Kooij, F. M.; Lekkerkerker, H. N. W. *J. Phys.: Condens. Matter* **1996**, *8*, 9451.
(73) van Bruggen, M. P. B.; Lekkerkerker, H. N. W. *Langmuir* **2002**, *18*, 7145.

MA061603J